

REPORTS

focusing the light onto the core region, but they were always accompanied by substantial light that filled the whole fiber. No indication of a far-field pattern like that in Fig. 4B was observed. A relatively sharp transition—with wavelength—from a confined to a nonconfined mode is expected to be a feature of this type of waveguiding.

Some qualitative insight into the nature of the guided modes being described here can be gained by considering the honeycomb structure shown in Fig. 2 as a large number of independent silica strands that are strongly coupled together. Each isolated strand would support many distinct waveguide modes, each with a different value of β . When a large number of strands are placed in close proximity, they couple together, and each mode of the single strand opens up into a passband of modes of the

composite structure, each passband now covering a range of β values. The passbands are separated by band gaps. The central silica strand (the “core”), which has a large hole in the middle and six smaller interstitial holes disposed symmetrically around it, would, if isolated, support a different set of waveguide modes because of its different morphology. If the β value of one of these modes falls within one of the bands of modes of the periodic cladding, this mode of the core will be coupled to the extended modes of the periodic cladding. However, if one of the modes of the core region falls in between the passbands of the fully periodic cladding region, then this mode is localized within the core and forms a PBG guided mode. Thus, at some wavelengths, there is a mode trapped within the core (the “guided mode”), whereas at other wavelengths the modes are extended and fill the fiber. A possible reason for the importance of the hard-to-model interstitial holes within the core is that they will affect the β values of the core modes, drawing one of these into the band gap of the continuous material.

Band gap guided modes are expected to have quite different properties to the modes of conventional optical waveguides. For example, we observe that the fiber being described here is strongly birefringent, with a beat length on the order of millimeters (that is, the different polarization modes have rather different propagation constants). We conclude that small imperfections in the structure can have a large effect on the propagation constant of the trapped modes. The dispersion of these fibers is likely to be far

larger than that observed in any previous optical fiber waveguide for the correct choice of fiber design parameters. Other properties of these fibers (for example, their susceptibility to bend loss) remain to be investigated, and even more counterintuitive designs (a silica-air waveguide where the light is trapped within an air hole, for example) are possible. This is only the first of a very broad class of fiber guided modes, which show great technological promise and are of substantial scientific interest.

References and Notes

1. E. Yablonovitch, *J. Opt. Soc. Am. B* **10**, 283 (1993).
2. P. St. J. Russell, D. M. Atkin, T. A. Birks, P. J. Roberts, in *Microcavities and Photonic Bandgaps: Physics and Applications*, J. G. Rarity and C. Weisbuch, Eds. (Kluwer, Dordrecht, Netherlands, 1996), pp. 203–218.
3. T. A. Birks, P. J. Roberts, P. St. J. Russell, D. M. Atkin, T. J. Shepherd, *Electron. Lett.* **31**, 1941 (1995).
4. J. D. Joannopoulos, R. D. Meade, J. N. Winn, *Photonic Crystals: Molding the Flow of Light* (Princeton Univ. Press, Princeton, NJ, 1995).
5. J. C. Knight, T. A. Birks, P. St. J. Russell, D. M. Atkin, *Opt. Lett.* **21**, 1547 (1996) [errata: *ibid.* **22**, 484 (1997)].
6. T. A. Birks, J. C. Knight, P. St. J. Russell, *ibid.*, p. 961.
7. J. C. Knight, T. A. Birks, P. St. J. Russell, J.-P. de Sandro, *J. Opt. Soc. Am. A* **15**, 748 (1998).
8. J. C. Knight, T. A. Birks, R. F. Cregan, P. St. J. Russell, J.-P. de Sandro, *Electron. Lett.* **34**, 1347 (1998).
9. R. J. Tonucci, B. L. Justus, A. J. Campillo, C. E. Ford, *Science* **258**, 783 (1992).
10. D. Cassagne, C. Jouanin, D. Bertho, *Phys. Rev. B* **53**, 7134 (1996).
11. J. Broeng et al., *Opt. Commun.* **156**, 240 (1995).
12. Supported by the Defence Evaluation and Research Agency, Malvern, UK, and the UK Engineering and Physical Sciences Research Council. Donation of fiber-drawing equipment from BT Research Laboratories, Martlesham, UK, is gratefully acknowledged.

25 August 1998; accepted 14 October 1998

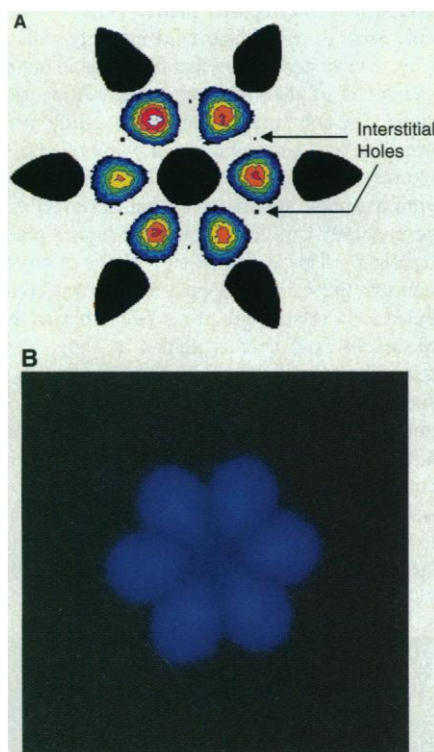


Fig. 4. Near- and far-field patterns observed with laser light (wavelength = 458 nm) to excite the guided mode in a 50-mm length of fiber. (A) A contour map of the observed near-field pattern (color) superimposed on a scanning electron micrograph showing the fiber morphology (black). The interstitial holes in the structure (which appear between the lobes of the guided mode) are clearly visible. The guided-mode field intensity outside the first ring of air holes is at least two orders of magnitude less than the peak intensity shown. (B) A photograph of the observed far-field pattern. The pattern was recorded by allowing the diffracting light emerging from the end of the fiber to fall onto a paper screen, which was then imaged onto photographic film from the back. The orientation of the six main lobes in the far-field pattern is the same as those in the near field.

Direct Demonstration of Milk as an Element of Archaeological Economies

Stephanie N. Dudd and Richard P. Evershed*

The stable carbon isotope ($\delta^{13}\text{C}$) compositions of individual fatty acid components of remnant fats preserved in archaeological pottery vessels show that dairying was a component of archaeological economies. Characteristic $\delta^{13}\text{C}$ values arise from biases in the biosynthetic origins of the $\text{C}_{18:0}$ fatty acids in milk and adipose fat. Milk and adipose fat from animals raised on similar pastures and fodders have distinct isotopic signatures.

Although sheep are thought to have been domesticated in the Near East at ~9000 B.C. and cattle and goats were domesticated at ~7000 B.C., there is no direct evidence that they were milked. Pictorial and written

records from the Sahara, Egypt, and Mesopotamia show that dairying had begun there by 4000 to 2900 B.C. (1). Evidence of dairying during the prehistoric period in Britain has been limited solely to secondary evidence associated with the procurement and use of dairy products, such as putative ceramic “cheese” strainers, dating from 4500 B.C. (2, 3). Faunal studies have suggested that a high neonatal cull and a bias in the adult cull in domestic ruminant animals may indicate dair-

Organic Geochemistry Unit, School of Chemistry, University of Bristol, Cantock's Close, Bristol, BS8 1TS, UK.

*To whom correspondence should be addressed. E-mail: r.p.evershed@bristol.ac.uk

ying (4, 5). Here we provide direct evidence of dairying from preserved residues of dairy products themselves.

Degraded animal fats are the most common class of organic residue observed in archaeological ceramics (6–9), identified by characteristically high abundances of saturated fatty acids, particularly palmitic (C_{16:0}) and stearic (C_{18:0}) acids. We have searched for these residues in more than 1000 potsherds from sites throughout Europe dating from the Neolithic through Bronze and Iron Age, Roman, Saxon, and medieval periods, using gas chromatography (GC) and GC–mass spectrometry (GC/MS) techniques. Most of the vessels correspond to those generally associated with food processing or storage (that is, jars and bowls), recovered from domestic areas of settlements. More than 40% of all sherds studied yielded appreciable lipid residues (10–13). Although there is no problem in detecting degraded animal fats, identifying the origin of the fats or specifying whether they are mixtures of fats from different species is much more problematic. A number of chemical criteria can be used to distinguish between the residues of animal fats preserved in archaeological pottery (13), including (i) the positional isomers of monounsaturated fatty acids; (ii) the abundances of odd-carbon-number (C_{15:0} and C_{17:0}) *iso*- and *anteiso*-branched-chain fatty acids; (iii) fatty acid and triacylglycerol distributions; and (iv) the $\delta^{13}\text{C}$ values of the major saturated fatty acids C_{16:0} and C_{18:0}, determined by GC–combustion-isotope ratio MS [GC–C–IRMS (13, 14)]. Bulk stable isotope studies allow the detection of remnant fats in carbonized food residues from archaeological sites (15, 16), but compound-specific $\delta^{13}\text{C}$ measurements can allow the fats from ru-

minant and nonruminant animals to be distinguished (13).

One major category of fat that we should be able to detect in pottery vessels is that derived from milk (for example, butterfat). Just as with the adipose fats, the processing of milk by pasteurizing or cooking, involving milk or butter, would result in the absorption of appreciable quantities of fat into the walls of unglazed pottery vessels. Fresh milk fats differ from adipose fats in their fatty acid composition because of the presence of short-chain (C₄ to C₁₄) saturated fatty acids (17). However, even though it is known that dairying was widely practiced in the Roman and later periods, we have consistently failed to detect fatty residues containing these characteristic shorter-chain fatty acids in lipid extracts from pottery vessels.

Because dairy products must have been processed in pottery vessels (18, 19), our apparent inability to detect dairy fats must stem from compositional alteration through decay during burial. As a test, we examined the triacylglycerol distributions of milk fat from fresh milk and of

ruminant adipose fat after decay in the laboratory when absorbed into unglazed replica ceramic sherds (Fig. 1). Over a short time, the distribution of lipid components in milk transformed into a distribution more closely resembling that of the adipose fat through preferential hydrolysis of the short-chain acyl moieties as a result of reduced steric effects at ester linkages in triacylglycerols as compared with their long-chain counterparts (20). Once released from triacylglycerols by hydrolysis, the short-chain fatty acids are appreciably more water soluble (and volatile) than their long-chain counterparts (21). This experiment confirms that selective decay of milk lipids leads to a distribution of fatty acids resembling that of adipose fats. Hence, although the fats preserved in archaeological pottery in principle offer an excellent source of information concerning the exploitation of dairy products by early farmers, our ability to recognize them through chemical analysis has been thwarted because of diagenetic alteration during burial.

The $\delta^{13}\text{C}$ values are diagnostic, however. We analyzed by GC–C–IRMS fats extracted from

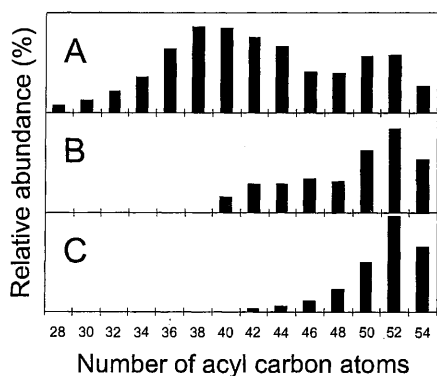


Fig. 1. Triacylglycerol distributions in (A) fresh milk, (B) milk absorbed in an unglazed potsherd and degraded in the laboratory under oxic conditions for 90 days, and (C) fresh ruminant (ovine) adipose fat. The distributions were determined by high-temperature GC of total lipid extracts (23). Clean replica potsherds (approximately 2 g) were soaked in solutions of White goat milk, with absorption facilitated by ultrasonication (2 by 20 min). Potsherds were dried to constant weight at room temperature before burial in flasks of mushroom compost. The flasks were plugged with extracted cotton wool to allow diffusion of air and then incubated at 30°C.

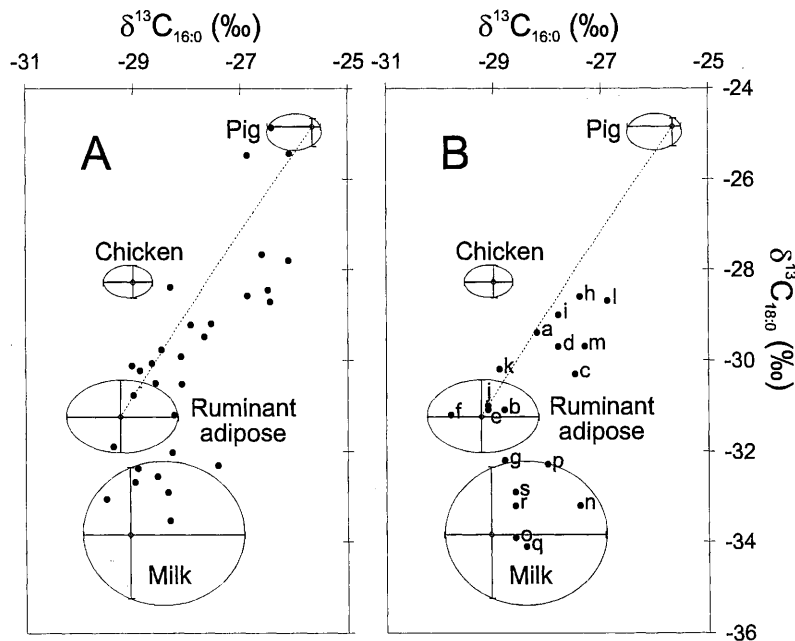


Fig. 2. Plot of the $\delta^{13}\text{C}$ values of the major *n*-alkanoic acid components (C_{16:0} and C_{18:0}) of the lipid extracts from potsherds from (A) West Cotton (late Saxon to early medieval) and (B) Stanwick (Iron Age–Romano-British). The archaeological fats (solid circles) cluster near the reference adipose and milk fats (bovine and ovine). In the case of West Cotton, nonruminant (porcine) adipose fats have also been identified. The mixing curves (dashed lines) have been calculated (25) to illustrate the $\delta^{13}\text{C}$ values that would result from the mixing of ovine/bovine and porcine fats in the vessels. The encircled fields encompass the ranges for reference animal fats, with the ranges crossing at the arithmetic mean. The numbers of different reference fats analyzed were as follows: pig adipose fat, 4; ruminant adipose fat, 9 (3 cow and 6 sheep); chicken adipose fat, 8; milk fat, 7 (6 cow and 1 sheep). All the animals were raised on C₃ diets. The more depleted $\delta^{13}\text{C}$ values for the C₁₈ fatty acid in the milk fats arises through routing of a large proportion of fatty acids directly from the diet (after biohydrogenation) to milk production. The $\delta^{13}\text{C}$ values for the fatty acids in the reference fats have been corrected for the post-Industrial Revolution effects of fossil fuel burning, which has decreased the $\delta^{13}\text{C}$ value of atmospheric CO₂ by 1.2‰ since the middle of the 19th century (26). The letters adjacent to the points in (B) correlate with the triacylglycerol distributions shown in Fig. 3 and correspond to the following types of domestic archaeological vessels: a, b, e, f, h through m, p, r, and s are jar-form vessels of various sizes; c is a mortar; d is a ceramic lid; g and n are flanged and wide bowls, respectively; and i, o, and q are small dishes. There was no obvious correlation between vessel form and the type of fat they contained. Analytical precision is $\pm 0.3\%$.

pottery vessels recovered from the late Saxon to early medieval site of West Cotton, Northamptonshire, UK, and from the Iron Age–Romano-British site of Stanwick, also in Northamptonshire, and compared the results with those from ruminant and nonruminant modern reference fats (Fig. 2). At West Cotton (Fig. 2A), the archaeological fats cluster in the range of the ruminant and nonruminant reference fats, whereas the extracts from Stanwick (Fig. 2B) are biased toward ruminant fats, and several analyses indicate mixtures of ruminant and nonruminant adipose fats and appear to show that different fats were processed in the same vessels.

In several of the ancient fats, the $C_{18:0}$ fatty acid is depleted in ^{13}C as compared with the other remnant fats obtained from the archaeological vessels. Consideration of the biochemistry and physiology of milk production in ruminant animals (17, 22) and subsequent analysis of reference milk fats obtained from sheep and cattle reared on a C_3 pasture indicate that these ^{13}C -depleted fatty acids originate from milk fat. The $\delta^{13}C$ values for the reference milk fats plot close to the values obtained for the archaeological fats containing the more depleted C_{18} fatty acids.

The distinctive trends seen in the $\delta^{13}C$ values of the dairy product $C_{16:0}$ and $C_{18:0}$ fatty acids reflect their different biosynthetic origins. The $C_{16:0}$ component in milk is synthesized

largely in the mammary gland de novo from acetate (derived mainly from dietary carbohydrate). The $C_{18:0}$ component derives in part directly from the dietary fatty acids, mainly $C_{18:2}$ and $C_{18:3}$, by biohydrogenation (bacterial reduction) in the rumen and in part from other sources, such as mobilization of adipose fatty acids (Fig. 3). During lactation, it has been found that ~40% of milk fat is derived directly from absorbed dietary fatty acids, corresponding mainly to C_{18} components (17, 22). In ruminant adipose fats, the $C_{16:0}$ and $C_{18:0}$ fatty acids are also derived from a combination of dietary lipids and de novo synthesis; however, the enhanced routing of dietary fatty acids directly to milk during lactation gives rise to the more negative $\delta^{13}C$ values for the $C_{18:0}$ fatty acid of milk fat as compared with the adipose fat of animals feeding on the same diets. The more negative $\delta^{13}C$ values [~–32.5 to –35 per mil (‰)] seen for $C_{18:0}$ in milk is similar to the depleted values recorded for the major unsaturated C_{18} fatty acids in pastures and fodders: –35‰ (the weighted mean for C_{18} fatty acids in grass). Thus, our data show that milk and adipose fats from animals raised on similar diets are separable on the basis of the comparison of the $\delta^{13}C$ values of $C_{16:0}$ and $C_{18:0}$ fatty acids and that this provides the basis for determining the presence of milk fat in archaeological pottery. The trend is seen for both cows and sheep

because the mean value obtained for the reference cows' milk $C_{18:0}$ fatty acid was –34‰ and that of the sheep's milk was –33.8‰.

The triacylglycerol distributions (Fig. 3), derived by high-temperature GC (23), for the extracts in Fig. 2B provide further information. Those displaying the heavier $\delta^{13}C$ values for their C_{18} fatty acids more closely resemble the distribution characteristic of fresh adipose fat (Fig. 1C) than that of either fresh (Fig. 1A) or degraded (Fig. 1B) milk fat. The distributions for the vessels yielding the lighter $\delta^{13}C$ values show a remarkably close correspondence to the laboratory-degraded milk fat (Fig. 1B). Although the triacylglycerol distributions support the isotopic differences between the various animal fats, the $\delta^{13}C$ values offer a more robust criterion because intact triacylglycerols are frequently not preserved in ancient pottery as they are completely hydrolyzed to their component free fatty acids.

Because the trends seen in the $\delta^{13}C$ values of the individual fatty acid components of animal fats reflect the fundamental difference in the $\delta^{13}C$ values of the fatty acids and carbohydrate components (~5‰) of typical forage and fodder materials (24), this method can be applied at any archaeological site.

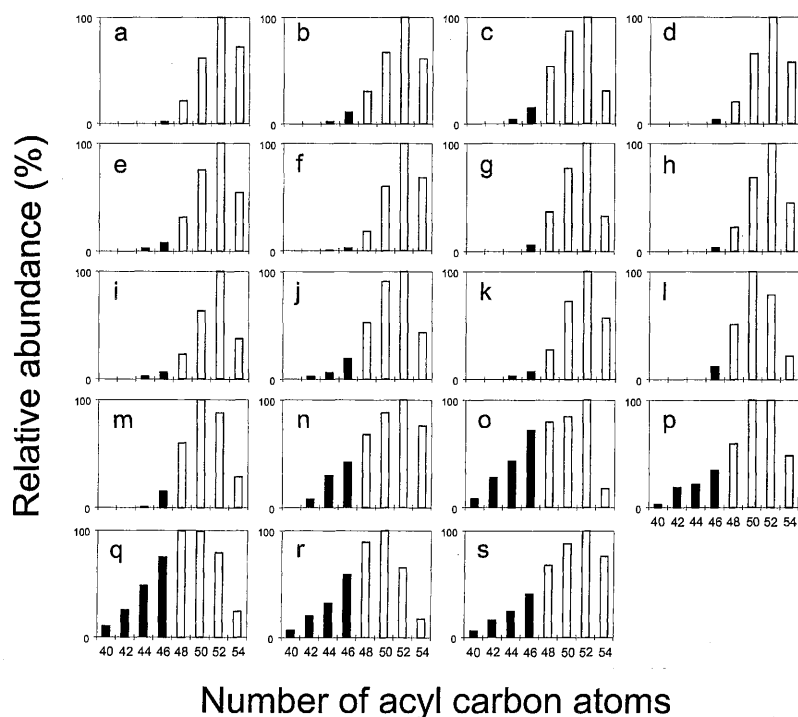


Fig. 3. Histograms showing the distributions of triacylglycerols of equal carbon number in total lipid extracts from potsherds from the Iron Age–Romano-British vessels recovered from excavations at Stanwick. Distributions a through m correspond to those displaying $\delta^{13}C$ values characteristic of ruminant adipose fats, whereas n through s correspond to those displaying $\delta^{13}C$ values characteristic of milk fat. The identification of the origins of these fats is supported by comparison with the triacylglycerol distributions, notably the higher abundance of C_{40} to C_{46} components (solid bars), which characterize degraded milk fat (compare with Fig. 1B).

References and Notes

1. F. J. Simoons, *Anthropos* **74**, 61 (1979).
2. A. Sherratt, in *Pattern of the Past: Studies in Honour of David Clarke*, I. Hodder, G. Isaac, N. Hammond, Eds. (Cambridge Univ. Press, Cambridge, 1981), pp. 261–305.
3. G. W. W. Barker, *Landscape and Society: Prehistoric Central Italy* (Academic Press, London, 1981).
4. A. J. Legge, in *Farming Practice in British Prehistory*, R. Mercer, Ed. (Edinburgh Univ. Press, Edinburgh, 1981).
5. P. Crabtree, *Expedition* **28**, 59 (1987).
6. R. E. Jones, *Greek and Cypriot Pottery: A Review of Scientific Studies* (Occasional Paper no. 1, British School at Athens at Fitch Laboratory, Athens, Greece, 1986).
7. R. C. A. Rottländer, *Archaeo-Physika* **12**, 1 (1990).
8. C. Heron and R. P. Evershed, in *Archaeological Method and Theory* **5**, M. Schiffer, Ed. (Univ. of Arizona Press, Tucson, AZ, 1993), pp. 242–284.
9. S. Needham and J. Evans, *Oxf. J. Archaeol.* **6**, 21 (1987).
10. S. Charters, R. P. Evershed, L. J. Goad, P. W. Blinkhorn, V. Denham, *Archaeometry* **35**, 211 (1993).
11. R. P. Evershed, C. Heron, S. Charters, L. J. Goad, *Proc. Br. Acad.* **77**, 187 (1992).
12. R. P. Evershed et al., *Tetrahedron Lett.* **36**, 8875 (1995).
13. R. P. Evershed et al., *Naturwissenschaften* **84**, 402 (1987).
14. R. P. Evershed, K. I. Arnot, J. Collister, G. Eglinton, S. Charters, *Analyst* **119**, 909 (1994).
15. C. A. Hasdorf and M. J. DeNiro, *Nature* **315**, 489 (1985).
16. B. L. Sherriff, M. A. Tisdale, B. G. Sayer, H. P. Schwarcz, M. Knyf, *Archaeometry* **37**, 95 (1995).
17. W. W. Christie, *Lipid Metabolism in Ruminant Animals* (Pergamon, Oxford, 1981), pp. 203–226.
18. Ph. Gouin, *Paléorient* **16**, 37 (1990).
19. J. Podolák, *Ethnol. Slav.* **16**, 49 (1984).
20. A. K. Balls, M. B. Matlack, I. W. Tucker, *J. Biol. Chem.* **121**, 125 (1937).
21. F. D. Gunstone, J. L. Harwood, F. B. Padley, Eds. *Lipid Handbook* (Chapman & Hall, London, 1986), pp. 353–354.
22. P. McDonald, R. A. Edwards, J. F. D. Greenhalgh, *Animal Nutrition* (Longman, Essex, UK, 1988).

23. R. P. Evershed, C. Heron, L. J. Goad, *Analyst* **115**, 1339 (1990).
 24. P. Deines, in *Handbook of Environmental Isotope Geochemistry*, P. Fritz and J. C. Fontes, Eds. (Elsevier, Amsterdam, 1980), pp. 329–406.
 25. S. E. Woodbury, R. P. Evershed, J. B. Rossell, R. E. Griffiths, P. Farnell, *Anal. Chem.* **67**, 2685 (1995).
 26. H. Friedli, H. Lotscher, H. Oeschger, U. Siegenthaler, B. Stauffer, *Nature* **324**, 237 (1986).

27. We thank J. Ridge and L. Ridge for their help in providing reference fats, J. Carter and A. Gledhill for technical support, the National Environment Research Council (grant GR3/10153) for funding and MS facilities (grant F14/6/13), and English Heritage and the Northamptonshire County Archaeology Unit for archaeological samples.

3 August 1998; accepted 6 October 1998

Pb Isotopic Variability in Melt Inclusions from Oceanic Island Basalts, Polynesia

A. E. Saal, S. R. Hart, N. Shimizu, E. H. Hauri, G. D. Layne

Previous studies have suggested that melting processes are responsible for the trace element variability observed in olivine-hosted basaltic melt inclusions. Melt inclusions from three individual lava samples (two from Mangaia, Cook Islands, and one from Tahaa, Society Islands) have heterogeneous Pb isotopic compositions, even though the erupted lavas are isotopically homogeneous. The range of Pb isotopic compositions from individual melt inclusions spans 50 percent of the worldwide range observed for ocean island basalts. The melt inclusion data can be explained by two-component mixing for each island. Our data imply that magmas with different isotopic compositions existed in the volcanic plumbing system before or during melt aggregation.

Studies of oceanic basalts have shown that the mantle is isotopically heterogeneous (1). However, the nature, distribution, and scale of these heterogeneities remain problematic. The aggregation of melts on their way to the surface, and mixing in magma chambers before eruption, can obscure the chemical and isotopic signatures of preaggregated melts. Trace and major element studies of olivine-hosted melt inclusions have been successful in defining the chemical composition of preaggregated melts. However, the lack of isotopic information in melt inclusions has made it difficult to distinguish whether these melt compositions represent different extents of melting from a single source (2) or originate from different source compositions. Here we present a study of Pb isotopes of melt inclusions from three geochemically well-characterized basalt samples (3, 4) (two from Mangaia, Cook Islands, and one from Tahaa, Society Islands chain) that reveal a large range in Pb isotopic values. The isotopic compositions of bulk samples from the Mangaia and Tahaa islands are very similar to two separate mantle compositions known as the HIMU (high-U/Pb mantle) and EMII (enriched mantle 2) end members, respectively (5). The major and trace element compositions of these lavas have been explained as resulting from melting from a single mantle source containing

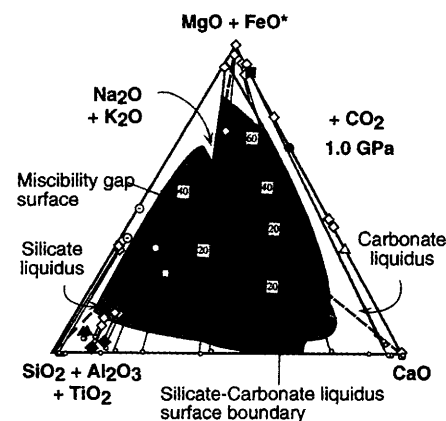
some recycled oceanic crust (6).

We recovered olivine (Fosterite content ranging from 84 to 89%) and clinopyroxene-hosted melt inclusions from two primitive basalts from Mangaia (olivines and clinopyroxenes from sample MGA-B-25, ankaramite; and olivines from sample MGA-B-47, picrite). Many of the inclusions now contain Ti-augite, Cr-spinel, ilmenite, kaersutite, sphene, apatite, and phlogopite that crystallized after entrapment of the melt (7) (see supplementary data in Table W1 at www.sciencemag.org/feature/data/984333.shl). Some melt inclusions (~7%) from both samples contain coexisting silicate glasses,

sulfide, and carbonate globules. These phases provide direct evidence for the existence of carbonate-rich magmas in the Cook-Austral chains, as inferred from studies of mantle xenoliths from Tubuaii (8), and of Zr/Hf fractionation in Mangaia whole-rock basalts (9). The carbonate spherules consist largely of calcium-magnesium-iron carbonate with minor alkali contents and are associated with Ca- or Mg-rich volatile-bearing silicate glasses or cryptocrystalline ground mass (up to 15% volatiles) and phonolitic glasses (Table W1). The major element compositions of the carbonates and silicate glasses from Mangaia are similar to those reported for metasomatized mantle xenoliths (for example, Spitsbergen) (10) and are inconsistent with the experimental data for liquid immiscibility (11) (Fig. 1). The phase relations shown in Fig. 1 indicate that none of the Mangaia silicate glass and carbonate globule compositions from the melt inclusions represent equilibrium immiscible liquids; they are too far removed from the miscibility gap, well inside the forbidden volumes of the primary silicate and carbonate liquidus, respectively (11). Previous work on carbonate-bearing mantle xenoliths suggested that dolomite and magnesian calcite represent primary melts, calcite is a solid phase crystallizing from a carbonated silicate melt, and amorphous magnesite-ankerite phases are formed as a result of the breakdown of primary carbonate minerals (10, 11). Mangaia silicate glasses record a complex history of crystal fractionation and probably in some cases (Mg-rich volatile-bearing glasses) decompression-induced dissolution or reaction of previously crystallized phases in volatile-rich melt inclusions (8, 10, 11). The carbonate observed in Mangaia melt inclusions crystallized from a primitive CO₂-rich magma in the lithosphere at pressures lower than 2.5 GPa.

The silicate glasses and carbonate globules from the Mangaia melt inclusions have a range

Fig. 1. (SiO₂ + Al₂O₃ + TiO₂) – (MgO + FeO*) – (CaO) – (Na₂O + K₂O) in a percent-by-weight-generalized pseudoquaternary phase diagram at 1.0 GPa (10), showing the major element composition of silicate glasses and carbonate globules from Mangaia melt inclusions and from Spitsbergen mantle xenoliths (9). The figure shows the three major liquidus volumes (the miscibility gap and the silicate and carbonate liquidus fields) and the liquidus surfaces between them. Contours and values for (MgO + FeO*) of the surfaces are also shown as boxed numbers. Solid triangles, glass 1; solid diamonds, glass 2; dotted circle, glass 3; solid square, solid circle, and open triangle, carbonate globules; open diamonds, silicate glasses and carbonate globules from Spitsbergen xenoliths (9); open circle and open square, whole-rock lavas from Mangaia (MAG-B-47 and MAG-B-25, respectively) (4). The small circles are the projections of each point from the (MgO + FeO*) vertex onto the basal plane of the tetrahedron. The composition of the Mangaia silicate glasses and carbonate globules is very similar to the composition of those found in Spitsbergen xenoliths. The phase relationships at 1.0 GPa (also at 2.5 GPa, not shown in figure) indicate that none of these carbonate compositions represent equilibrium-immiscible liquids. See Table W1 for supplementary data.



A. E. Saal, S. R. Hart, N. Shimizu, G. D. Layne, Department of Geology and Geophysics, Woods Hole Oceanographic Institution, Woods Hole, MA 02543, USA. E. H. Hauri, Department of Terrestrial Magnetism, Carnegie Institution of Washington, 5241 Broad Branch Road, N.W., Washington, DC 20015, USA.